Applied Surface Science 724 (2026) 165776

Contents lists available at ScienceDirect

Applied Surface Science

journal homepage: www.elsevier.com/locate/apsusc

Full Length Article

Boron-irradiated Si_3N_4: the origin of the defect responsible for the red shift of fundamental absorption edge and increase of refractive index

V.A. Gritsenko [a,b], T.V. Perevalov [a], Yu.N. Novikov [a,*], A.A. Gismatulin [a]

[a] Rzhanov Institute of Semiconductor Physics SB RAS, 13 Lavrentiev Aven., 630090 Novosibirsk, Russia
[b] Novosibirsk State Technical University, 20 Marx Aven., 630073 Novosibirsk, Russia

ARTICLE INFO

Keywords:
Silicon nitride
Defect
X-ray photoelectron spectroscopy
Infrared absorption
Refractive index

ABSTRACT

The atomic structure of amorphous silicon nitride (Si_3N_4) irradiated with different doses of boron (B^+) ions and with energy 100 keV is studied using photoelectron spectroscopy and infrared absorption. Irradiation with B^+ ions leads to the broadening of the atomic Si 2s level toward lower energies, which indicates the formation of silicon–silicon (Si–Si) bonds. The dispersion of the refractive index of irradiated Si_3N_4 is studied experimentally and using quantum chemical modeling. The refractive index of Si_3N_4 increases upon irradiation with B^+ ions. Irradiation with B^+ ions is accompanied by a red shift of the fundamental absorption edge of Si_3N_4. This effect is explained by a shift of the edges of the conduction band and valence band toward the middle of the forbidden band due to the splitting of bonding and antibonding orbitals of Si–Si bonds with an increase in their concentration. The increase in the refractive index and the red shift of the fundamental absorption edge of Si_3N_4 irradiated with B^+ ions are due to the formation of radiation defects, that is Si–Si bonds.

1. Introduction

The charge-carrier sign (electrons or holes) and the conductivity of semiconductors are controlled by doping with donors which supply mobile electrons, or acceptors which supply mobile holes. One of the effective methods of doping semiconductors is ion implantation. As a rule, ion implantation is carried out through a dielectric, silicon oxide (SiO_2), or silicon nitride (Si_3N_4). The ion energy during implantation is about a hundred electron-volts. During implantation, radiation defects are formed in the dielectric, which are eliminated by a subsequent annealing.

Amorphous silicon oxide SiO_2 and amorphous silicon nitride Si_3N_4 are two key dielectrics in semiconductor devices. Thermal SiO_2 on silicon has a low density of surface states, low density of traps in the bulk and, therefore, is used as a gate dielectric in silicon field-effect transistors [1]. Si_3N_4, on the contrary, has a high concentration (10^{18}–10^{21} cm^{-3}) of deep (≈1.5 eV) electron and hole traps [1,3]. The nature of traps (their atomic and electronic structure) in Si_3N_4 is a subject of intense discussions [1–19]. The polaron and bipolaron nature of traps is discussed in [3]. Undercoordinated and overcoordinated atoms of silicon and nitrogen are considered in [1,15–19]. Paramagnetic defects are considered as traps [4–6]. The polaron model of the diamagnetic Si–Si bond [9–13] and impurity atoms of aluminum or oxygen are considered [14].

Si_3N_4 has a memory effect – the ability to localize electrons and holes injected into it with a giant lifetime in a localized state (10 years at 85 °C) and is used in TANOS (TaN-Al_2O_3-Si_3N_4-SiO_2-Si) charge trap flash (CTF) memories [20,21]. The non-volatile Resistive Random Excess Memory (ReRAM) is being developed based on silicon nitride. Such memory, compared to CTF, has a high (~10^9) number of reprogramming cycles and high performance in the reprogramming mode (~100 ns) [22]. Both stoichiometric Si_3N_4 [23] and ion-implanted Si_3N_4 [24] are used as an active medium in ReRAMs. To understand the physics of flash memory devices and ReRAM, it is important to establish the nature of the defects responsible for the memory properties of Si_3N_4.

In [25], the fundamental absorption edge of amorphous Si_3N_4 irradiated with neon ions and obtained by the Low Pressure Chemical Vapor Deposition (LPCVD) method was studied. It was found that the fundamental absorption edge shifts toward lower energies, depending on the synthesis technology, by 0.5–1.0 eV. Annealing at 700 °C leads to the reverse shift of the absorption edge toward higher energies. In [25], it is indicated that the shift of the absorption edge upon irradiation is due to the disorder in the silicon nitride structure. However, the nature (atomic structure) of the defects responsible for the shift of the absorption edge

* Corresponding author.
E-mail address: nov@isp.nsc.ru (Yu.N. Novikov).

https://doi.org/10.1016/j.apsusc.2025.165776
Received 15 July 2025; Received in revised form 9 December 2025; Accepted 29 December 2025
Available online 30 December 2025

of irradiated Si_3N_4 has not been established. In [26], the charge accumulation and discharge in silicon nitride irradiated with boron and phosphorus ions in microelectromechanical systems is studied. The nature of the defects arising during irradiation was not studied.

The aim of this work is to study the effect of irradiation with B^+ ions on the optical properties of Si_3N_4, which are refractive index and fundamental absorption edge. Another aim is to establish the origin of defects responsible for the red shift of the absorption edge and the increase in the refractive index in B^+-irradiated amorphous Si_3N_4.

2. Experimental methodology and quantum chemical modeling

Amorphous Si_3N_4 films were synthesized from a mixture of silane SiH_4 and ammonia NH_3 at 850 °C, the ratio $SiH_4/NH_3 = 1/100$. To study the photoelectron spectra, 160 nm thick Si_3N_4 films were deposited on n-type silicon with the (100) orientation. For optical measurements, Si_3N_4 was deposited on sapphire substrates. The thickness and refractive index were measured using an ellipsometer at the wavelength of 632.8 nm. Si_3N_4 was irradiated with 100 keV B^+ ions in the dose range from 3×10^{12} cm^{-2} to 3×10^{15} cm^{-2}. The annealing of irradiated Si_3N_4 was carried out in a nitrogen atmosphere at 700 °C for 30 min.

X-ray photoelectron spectra were measured using the SPECS's X-ray Photoelectron Spectra (XPS) machine with monochromatic Al Kα radiation (E = 1486.74 eV). Optical reflection and transmission spectra were measured on an SF-56 spectrometer, LOMO-Spectr, St. Petersburg, Russia. Infrared transmission spectra were measured on an FT-801 Fourier spectrometer, SIMEX, Russia.

The atomic and electronic structure of SiN_x was calculated within the density functional theory (DFT) in the periodic 3D cell model in the Quantum ESPRESSO package [27]. The exchange–correlation functional of the PBEsol parameterization, optimized norm-conserving Vanderbilt pseudopotentials and the cutoff energy of the plane-wave basis set of 70 Ry were used. The method used gives a Si_3N_4 bandgap value close to the experimental one, i.e. $E_g = 4.55$ eV. SiN_x ($x = 1.17$, 1.0, 0.83 and 0.67) structures were created by successive removals of various numbers of nitrogen atom pairs, followed by adding the corresponding number of hydrogen atoms for the charge neutralization in a 28-atom unit cell of α-Si_3N_4 (P31c). In [28], it was shown that the $SiL_{2,3}$ emission spectra of amorphous Si_3N_4 and α-Si_3N_4 have a similar shape. These data indicate that the electronic structure of these materials is similar. After full structural relaxation calculations of all possible combinations, SiN_x structures with the lowest total energy were selected. After the electronic structure calculation, the optical spectra and the total density of states (TDOS) spectra were simulated by using the *k*-point grid 8 × 8 × 8.

3. Distribution of boron and defects in irradiated Si_3N_4

The STRIM-2013 program was used to calculate the distribution of implanted B^+ in the Si_3N_4/Si-substrate system. The 160 nm thick Si_3N_4 layer was set with the density of 3.44 g/cm^3. The silicon substrate thickness was 500 nm. The implantation of 10,000 B^+ ions was calculated at the energy of 100 keV with the implantation angle of 0 degrees. The calculation results are shown in Fig. 1. The calculated boron ion tracks after the implantation are shown in Fig. 1a. For Fig. 1b and c, 10,000 boron ions were recalculated to the maximum dose of 3×10^{15} cm^{-2} from the experiment.

It is evident from the distribution of boron ions in Si_3N_4 after the ion implantation (Fig. 1b) that the bulk of the ions goes into the silicon substrate. The concentration of generated nitrogen vacancies, as a result of implantation, are shown in Fig. 1c; the bulk of the generated nitrogen vacancies recombine later, but some of them remain. When calculating the optical spectra, for simplicity, we assumed a uniform composition of the Si_3N_4 film after irradiation with B^+ ions.

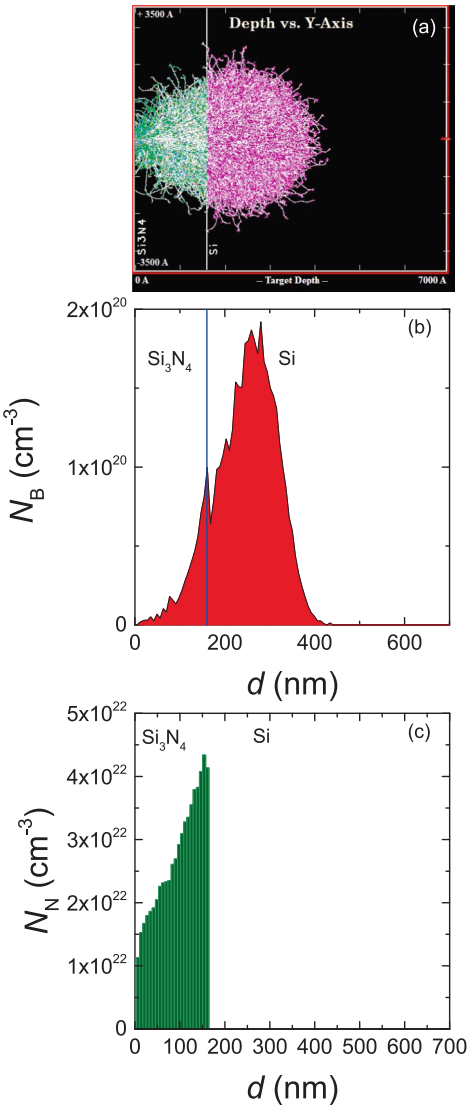

Fig. 1. (a) Calculated tracks of 10,000 B^+ ions in the Si_3N_4/Si structure. The track is white. The collision sites of the boron ion with nitrogen in Si_3N_4 is cyan. The collision sites of boron ion with Si in the substrate is magenta. (b) The distribution of B^+ in Si_3N_4 after ion implantation. (c) Generated N vacancies due to the implantation of B^+ ions. The implantation energy is 100 keV, and the maximum implantation dose is 3×10^{15} cm^{-2}.

4. Photoelectron spectroscopy of irradiated Si_3N_4

To establish the nature of the defects responsible for the low-energy shift of the fundamental absorption edge of irradiated Si_3N_4, the photoelectron spectra of the atomic Si 2s levels were studied (Fig. 2a).

The B^+ ion irradiation is accompanied by low-energy broadening of the Si 2s atomic level, similar to the case of the Si 2p atomic level in silicon nitride SiN_x enriched with excess silicon [29,30]. The low-energy broadening of the Si 2s level upon the B^+ ion irradiation indicates the formation of Si–Si bonds in implanted Si_3N_4. Fig. 2a are the experimental XPS spectra of the Si 2s atomic level of B^+ ion-irradiated Si_3N_4 and the original Si_3N_4 film, as well as the calculated Si 2s spectra of these materials. When calculating the Si 2s spectra of B^+ ion-irradiated Si_3N_4, it is assumed that five types of $SiN_\nu Si_{4-\nu}$ tetrahedra (where $\nu = 0$, 1, 2, 3, 4) contribute to the Si 2s spectrum. The indication $SiN_\nu Si_{4-\nu}$ means that, in the center of each tetrahedron, there is a Si atom surrounded by four N or Si atoms depending on the parameter ν. Five types of Gaussian tetrahedra with equidistant energy maxima are used. Using the results of

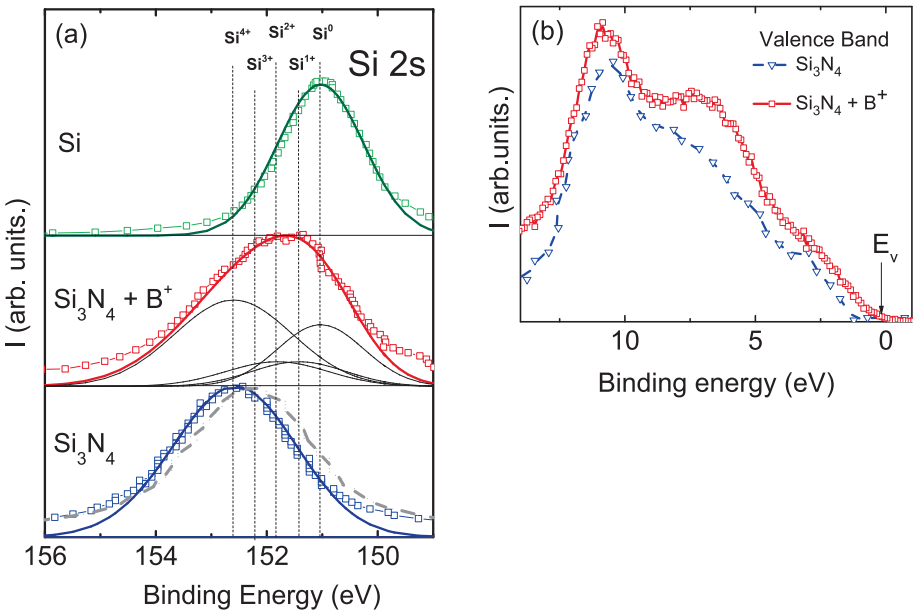

Fig. 2. Experimental XPS spectra: (a) of the level (squares) for ion-implanted Si and the initial Si_3N_4 film, and their deconvolution (solid lines). Notations Si^{4+}, Si^{3+}, Si^{2+}, Si^{1+} and Si^0 indicate the contributions to the Si 2s spectrum from five $SiN_\nu Si_{4-\nu}$ tetrahedra, where $\nu = 0, 1, 2, 3, 4$. The dotted line shows the Si 2s spectrum after irradiation and subsequent annealing. (b) Si_3N_4 valence band before irradiation (triangles) and after irradiation with B^+ ions (squares). The irradiation dose of Si_3N_4 with B^+ ions is 3×10^{14} cm^{-2}.

[31,32], the energy position (E_ν) and half-width (σ_ν) of the Si 2s state were determined for Si ($SiSi_4$ tetrahedron): $E_0 = 151$ and $\sigma_0 = 1.1$ eV; for Si_3N_4 (SiN_4 tetrahedron): $E_4 = 152.6$ and $\sigma_4 = 1.5$ eV [32]. The positions E_ν and half-widths σ_ν of the intermediate, three Gaussian functions of the Si 2s states ($\nu = 1, 2, 3$) for the SiN_3Si SiN_2Si_2 $SiNSi_3$ tetrahedra were determined by the linear interpolation of the $E_0(\sigma_0)$, $E_4(\sigma_4)$ values using the number of silicon atoms as a parameter. Using the given basis of five Gaussian functions, the experimental Si 2s spectrum of SiN_x can be decomposed as follows:

$$I(E) = \sum_{\nu=0}^{4} W_\nu \exp\left(-\frac{(E-E_\nu)^2}{2\sigma_\nu^2}\right) \quad (1)$$

where $I(E)$ is the calculated spectrum, E is the energy and W_ν is the contribution to the Si 2s spectrum from the $SiN_\nu Si_{4-\nu}$ tetrahedra, $\nu = 0$, 1, 2, 3, 4. The W_ν values were selected based on the best agreement between the calculated and experimental spectrum. The modeling of the Si 2s spectrum of implanted Si_3N_4 showed that the main contribution to the Si 2s spectrum is made by the tetrahedra $SiSi_4$, $SiSi_1N_3$, $SiSi_2N_2$, and SiN_4 (Fig. 2a). Thus, the results of photoelectron spectroscopy indicate that Si–Si bonds are formed when Si_3N_4 is irradiated. The experimental XPS spectra of the Si_3N_4 valence band, before irradiation [9] (triangles) and after irradiation (squares) with B^+ ions (dose 3×10^{14} cm^{-2}), are shown in Fig. 2b. After irradiation with B^+ ions, a shift of the valence band top to the middle of the band gap is observed, which indicates a decrease in the value of E_g.

5. Optical properties of irradiated Si_3N_4

The infrared transmission spectra of irradiated Si_3N_4 on a silicon substrate, before and after annealing, are shown in Fig. 3. Polar Si-N bonds with large dipole moments make the largest contribution to the spectra. Covalent Si-Si bonds in irradiated Si_3N_4 do not contribute to the infrared absorption, since the dipole moment of the Si-Si bond is zero. The stretching vibrations of the Si–N bond have a transmission minimum of about 850 cm^{-1} (≈12 μm), and the vibrations of the Si–N–Si bridge have a transmission minimum of about 430 cm^{-1} (≈23 μm). When Si_3N_4 was irradiated with B^+ ions, the transmission at 850 cm^{-1} and 430 cm^{-1} increased. An increase in the infrared transmission intensity for the stretching vibrations of the Si–N bonds in Si_3N_4 implanted

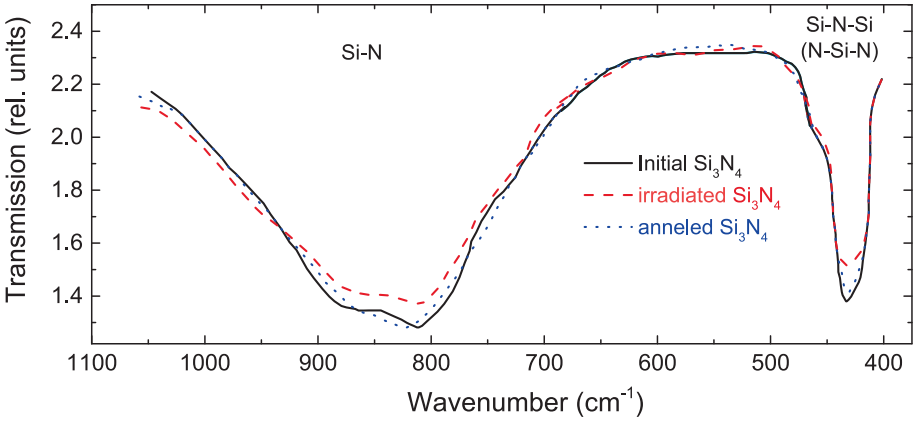

Fig. 3. Infrared transmission spectrum of the initial Si_3N_4, and Si_3N_4 films irradiated with B^+ ions (dose 3×10^{14} cm^{-2}) before and after a subsequent annealing.

with B^+ ions in Fig. 3 indicates the rupture of the Si–N bonds according to the reaction.

$$\equiv Si–N= \rightarrow \equiv Si\cdot + N= \quad (2)$$

As a result of the ≡Si–N= bond rupture, a triple-coordinated atom with an unpaired electron ≡Si and a double-coordinated nitrogen atom with an unpaired electron =N are formed. When irradiated, nitrogen atoms move into the interstitial space. It follows from Fig. 3 that when Si_3N_4 is irradiated with B^+ ions, approximately five percent of the Si–N bonds is ruptured according to reaction (2).

The annealing is accompanied by the return of the spectra to the initial state (Fig. 3). Such behavior of the infrared transmission spectra can be explained by the rupture of the Si–N bonds during the irradiation of Si_3N_4 and the subsequent restoration of the Si–N bonds during annealing. This phenomenon is discussed in the next paragraph.

The reflection spectra of Si_3N_4 irradiated with B^+ ions on silicon are shown in Fig. 4. The refractive index of the silicon substrate is greater than that of the Si_3N_4 film. For this case, the minimum in reflection (from the antireflection coating) is the minimum thickness, which is a multiple of a wavelength quarter:

$$n(\lambda) \bullet d = \frac{m+\frac{1}{2}}{2}\lambda \quad (3)$$

the maximum in reflection (minimum in transmission)

$$n(\lambda) \bullet d = \frac{m}{2}\lambda \quad (4)$$

where λ is the wavelength, m is the interference order, d is the Si_3N_4 thickness, which we determined using ellipsometry. Reflectance oscillations are due to interference. An increase in the B^+ ion irradiation dose is accompanied by a shift in the reflection maxima toward lower energies. The spectral dependence of the refractive index of Si_3N_4 irradiated with B^+ ions is shown in Fig. 5a. When Si_3N_4 is irradiated with B^+, an increase in the refractive index is observed. An increase in the irradiation dose is accompanied by an increase in the refractive index, similar to what is observed when non-stoichiometric SiN_x is enriched with excess silicon [33]. The increase in the film refractive index, as a result of irradiation, is most likely due to the process of creating a high concentration of Si–Si bonds in the film, which is equivalent to the formation of non-stoichiometric silicon-enriched silicon nitride SiN_x.

The $n(h\nu)$ spectra calculated within the DFT for silicon nitride with different levels of silicon enrichment show a similar pattern of curves, where the vertical shift of $n(h\nu)$ towards larger values is greater as the value of x = [N]/[Si] decreases (Fig. 5b). The lower the value of x is, the higher is the concentration of Si–Si bonds. The qualitative agreement between the experimental and theoretical $n(h\nu)$ spectra for energies up to 3 eV indicates that the irradiation of Si_3N_4 with B^+ ions leads to the formation of a high concentration of Si–Si bonds. Thus, in terms of optical properties, stoichiometric Si_3N_4 films irradiated with B^+ ions are equivalent to non-stoichiometric silicon-enriched SiN_x films ($x < 4/3$). The discrepancy between the calculated and experimental curves (Fig. 5b) is expected and is explained by the use of bulk crystals in the simulations and a simplified approach for the dielectric functions calculation using the Random Phase Approximation (RPA) method. More accurate approaches, like using the time-dependent DFT (TD-DFT), or the Bethe-Salpeter equation, are too resource-intensive for such large atomic systems. The features of the *n(E)* spectra at energies above 3 eV for SiN_x ($x < 4/3$) can be explained by the corresponding optical transitions between occupied and unoccupied states near the valence band top and the conduction band bottom, as well as between defect levels within the bandgap (discussion below). Due to the use of a simple calculation model, a detailed analysis of these transitions was not conducted.

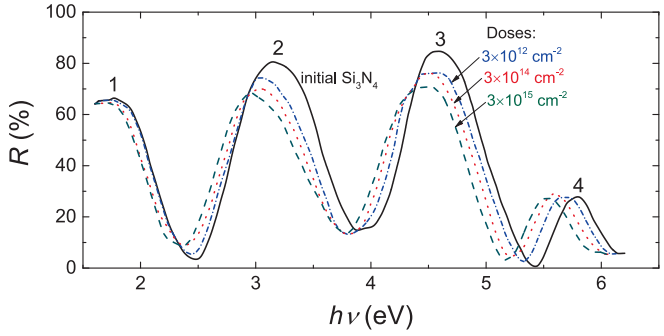

Fig. 4. Reflectance spectra of Si_3N_4 irradiated with B^+ ions on a silicon substrate. Initial and irradiated Si_3N_4 with the 100 keV B^+ ions implantation at the dose $D = 3 \times 10^{12}$ cm^{-2}, 3×10^{14} cm^{-2} and 3×10^{15} cm^{-2}. The numbers in the figure indicate the positions of the interference maxima.

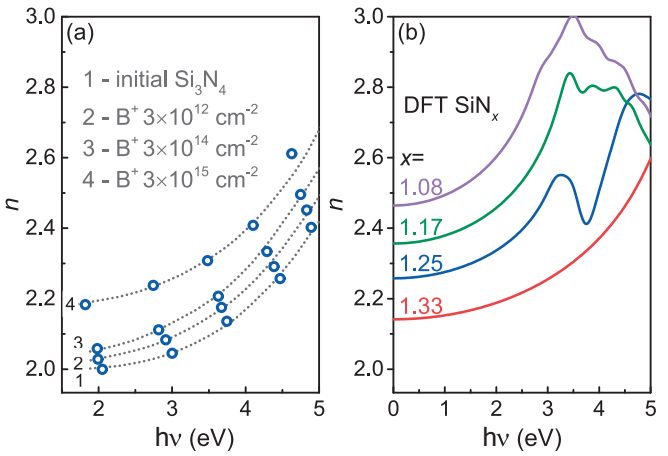

Fig. 5. Spectral dependence of the refractive index n of Si_3N_4 with different irradiation doses of B^+ ions (a); $n(h\nu)$ spectra calculated from first principles for SiN_x with different x values (b).

The transmission spectra of Si_3N_4 on a sapphire substrate irradiated with different doses of B^+ ions are shown in Fig. 6. When Si_3N_4 is irradiated with B^+ ions, a decrease in transmittance conditioned by the absorption due to the formation of Si-Si bonds is observed.

The irradiation with B^+ ions is accompanied by a decrease in the transmission of irradiated Si_3N_4 in the energy range of 3.5–6.0 eV. The spectral dependence of the fundamental absorption edge of the initial and irradiated Si_3N_4 film is shown in Fig. 7 The absolute accuracy of

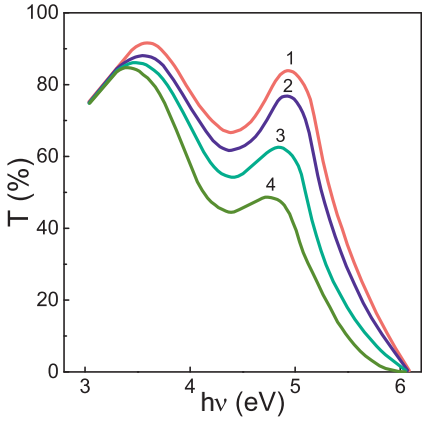

Fig. 6. Transmission spectra of Si_3N_4 (with thickness 160 nm) on a sapphire substrate irradiated with different doses of B^+ ions. 1- initial Si_3N_4, 2–4 – irradiation with B^+ ions: 2 – $D = 3 \times 10^{12}$ cm^{-2}, 3–3×10^{14} cm^{-2}, 4–3×10^{15} cm^{-2}.

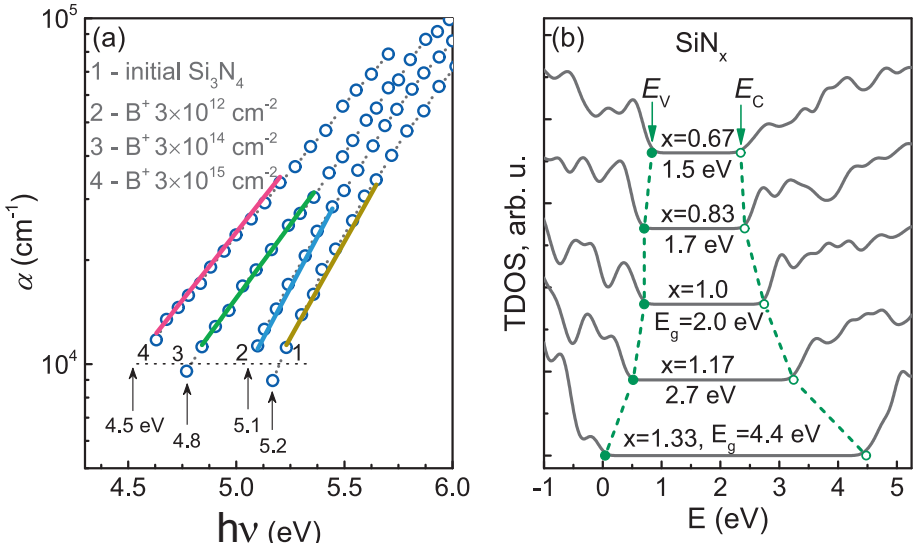

Fig. 7. Spectral dependence of the absorption coefficient of Si_3N_4 with different irradiation doses of B^+ ions (circles) and the calculated ones using the Urbach rule (solid lines) (a); Calculated TDOS spectra of SiN_x depending on the composition (b). The spectra are superimposed by the position of the N 2s peak 14.3 eV below E_V, and the E_V position of Si_3N_4 is taken as the zero energy. The energy values E_g for different values of x are presented in the figure.

determining the band gap width of irradiated Si_3N_4 in Fig. 7a is low (about 0.5 eV), but the relative accuracy of estimating E_g at a quantum energy corresponding to the absorption at the absorption coefficient of 10^4 is ≈0.1 eV. The optical absorption dispersion spectra α for silicon nitride films with different B^+ ion irradiation doses allow us to estimate from above the bandgap value as the photon energy at which α is 10^4 cm^{-1} (the so-called optical gap E_{04}) (Fig. 7a). It can be seen that, for the initial and irradiated films with doses of 3×10^{12} cm^{-2}, 3×10^{14} cm^{-2} and 3×10^{15} cm^{-2}, the E_{04} values are 5.2 eV, 5.1 eV, 4.8 eV and 4.5 eV, respectively. Thus, with an increase in the irradiation dose of the silicon nitride film with B^+ ions, a shift of the optical absorption edge to the long-wavelength region of the spectrum is observed. A similar decrease in the bandgap is observed with a decrease in the coefficient x = [N]/[Si] for SiN_x, as evidenced by the calculated TDOS (Fig. 7b).

This decrease is caused mainly by a shift of the conduction band edge E_C and the valence band top E_V into the bandgap. The SiN_x valence band top is formed mainly by atomic Si 3p orbitals corresponding to the bonding σ-orbitals of Si–Si bonds, and the shift of E_V toward higher energies is explained by an increase in the energy of these orbitals with an increase of nitrogen vacancies concentration (decrease in the parameter x value (Fig. 8)). The shift of E_C toward lower energies is explained by a decrease in the energy of the antibonding σ^*-orbitals of Si–Si bonds with an increase of the nitrogen vacancies concentration. The bonding and antibonding orbitals of the Si–Si bond are located near the top of the valence band and the bottom of the conduction band of Si_3N_4 [34,35]. An increase in the concentration of Si–Si bonds during irradiation, due to the removal of degeneracy, leads to a decrease in the bandgap of SiN_x and Si_3N_4 irradiated with B^+ ions (Fig. 8). Previously, a low-energy shift of the fundamental absorption edge was observed upon the irradiation of silicon nitride with neon ions and protons [25]. A similar low-energy shift of the fundamental absorption edge is observed upon the enrichment of nonstoichiometric SiN_x with silicon [29,30]. Also, we calculated optical absorption dispersion spectra (solid lines in Fig. 7a) using the Urbach rule [36]: $\alpha = \alpha_0 \times \exp((h\nu - E_{04})/E_U)$, where α_0 and E_U (Urbach energy) are model parameters. The agreement with the experiment was obtained with the following parameters: $\alpha_0 = 9.7 \times 10^3$ cm^{-1}, $E_U = 0.39$ eV for $E_{04} = 5.2$ and 5.1 eV; $E_U = 0.55$ eV for $E_{04} = 4.8$ and 4.5 eV. Calculations show that with an increase in the dose of irradiation of Si_3N_4 with B^+ ions, the value of E_U increases.

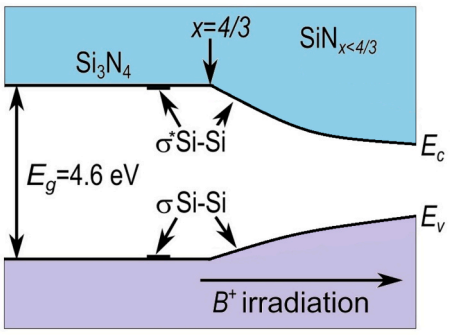

Fig. 8. Schematic representation of the reduction in the bandgap of SiN_x and irradiated Si_3N_4 due to the presence of Si–Si bonds.

6. Discussion of results

As a result of the rupture of the ≡Si–N= bond during irradiation, according to reaction (2), two intrinsic paramagnetic complementary defects are formed: a triple-coordinated silicon atom with an unpaired electron ≡Si· and a double-coordinated nitrogen atom with an unpaired electron =N. This is indicated by a decrease in the absorption coefficient of vibrational spectra in the infrared region of the spectrum. In work [37] it was shown that enrichment with silicon Si_3N_4 leads to a decrease in the absorption coefficient and a decrease in the gap value. The increase in the refractive index and the low-energy shift of the fundamental absorption edge of irradiated Si_3N_4, as quantum-chemical modeling indicates, are due to the formation of Si–Si bonds. The formation of Si–Si bonds in irradiated Si_3N_4 is directly indicated by the broadening of the Si 2s atomic level and the shift of the spectrum to the low-energy region, i.e. towards the silicon states in Fig. 2.

After the irradiation of Si_3N_4, the paramagnetic defects ≡Si and =N recombine in pairs according to reactions (3) and (4):

$$\equiv Si\cdot + \cdot Si\equiv \rightarrow \equiv Si\text{–}Si\equiv, \quad (5)$$

$$=N\cdot + \cdot N= \rightarrow =N\text{–}N=. \quad (6)$$

As a result of the recombination of paramagnetic ≡Si· and =N· defects in irradiated Si_3N_4, diamagnetic Si–Si and N–N bonds are formed. The formation of Si–Si bonds leads to a bandgap narrowing. The

spectral dependence of the absorption coefficient and quantum mechanical calculations confirms this. A decrease in the bandgap width with the increasing enrichment of SiN_x with silicon was observed in [38,39]. Also, the refractive index of Si in the IR region of the spectrum is ≈3.9 [40], while the refractive index of Si_3N_4 is ≈2 [41]. Therefore, an increase in the number of Si-Si bonds in SiN_x leads to an increase in its refractive index (Fig. 5). During the annealing of irradiated Si_3N_4, the interaction of Si–Si and N–N bonds takes place according to the reaction

$$\equiv Si–Si\equiv + =N–N= \rightarrow 2\equiv Si–N= \quad (7)$$

This is indicated by a decrease in the infrared transmittance of irradiated Si_3N_4 at 850 cm^{-1} during annealing (Fig. 3).

7. Conclusion

The effect of irradiation with B^+ ions on the structure and optical properties of amorphous Si_3N_4 was studied. Irradiation with B^+ ions leads to a red shift of the fundamental absorption edge and an increase in the refractive index of Si_3N_4. According to the quantum-chemical modeling, the red shift of the absorption edge and an increase in the refractive index during the irradiation with B^+ ions in Si_3N_4 are explained by the formation of intrinsic radiation defects, Si–Si bonds. Annealing leads to the recovery from radiation defects in irradiated Si_3N_4.

CRediT authorship contribution statement

V.A. Gritsenko: Writing – review & editing, Writing – original draft, Visualization, Validation, Methodology, Investigation, Conceptualization. **T.V. Perevalov:** Writing – review & editing, Visualization, Methodology, Formal analysis. **Yu.N. Novikov:** Writing – review & editing, Visualization, Methodology, Formal analysis. **A.A. Gismatulin:** Writing – review & editing, Visualization, Methodology, Formal analysis.

Funding

The work was supported by the Russian Science Foundation, grant N⁰ 25-12-00022.

Declaration of competing interest

The authors declare that they have no known competing financial interests or personal relationships that could have appeared to influence the work reported in this paper.

Acknowledgement

We are also thankful to Dr. V. A. Volodin for his discussion of this paper.

Appendix A. Supplementary data

Supplementary data to this article can be found online at https://doi.org/10.1016/j.apsusc.2025.165776.

Data availability

Data will be made available on request.

References

[1] S.M. Sze, Physics of Semiconductor Devices, John Wiley and Sons, Taiwan, 1981.
[2] L. Hückmann, J. Cottom, J. Meyer, Intrinsic charge trapping and reversible charge induced structural modifications in a-Si_3N_4, Adv. Phys. Res. 3 (2024) 2300109, https://doi.org/10.1002/apxr.202300109.
[3] C. Wilhelmer, D. Waldhör, L. Cvitkovich, D. Milardovich, M. Waltl, T. Grasse, Polaron formation in the hydrogenated amorphous silicon nitride Si_3N_4:H, Phys. Rev. B 110 (2024) 045201, https://doi.org/10.1103/PhysRevB.110.045201.
[4] W.L. Warren, P.M. Lenahan, Electron-nuclear double-resonance and electron-spin-resonance study of silicon dangling-bond center in silicon nitride, Phys. Rev. B 42 (1990) 1773–1780, https://doi.org/10.1103/PhysRevB.42.1773.
[5] W.L. Warren, P.M. Lenahan, S.E. Curry, First observation of paramagnetic nitrogen dangling-bond centers in silicon nitride, Phys. Rev. Let. 65 (1990) 207–210, https://doi.org/10.1103/PhysRevLett.65.207.
[6] W.L. Warren, J. Kanicki, J. Robertson, E.H. Poindexter, P.J. McWhorter, Electron paramagnetic resonance investigation of charge trapping centers in amorphous silicon nitride films, J. Appl. Phys. 74 (1993) 4034–4046, https://doi.org/10.1063/1.355315.
[7] J. Robertson, Electronic structure of silicon nitride, Philos. Mag. B 63 (1991) 47, https://doi.org/10.1080/01418639108224430.
[8] J. Robertson, Defects and hydrogen in amorphous silicon nitride, Philos. Mag. B 69 (1994) 307–326, https://doi.org/10.1080/01418639408240111.
[9] V.A. Gritsenko, J.B. Xu, I.H. Wilson, R.M. Kwok, Y.H. Ng, Short range order and nature of defects and traps in amorphous silicon oxynitride, Phys. Rev. Lett. 81 (5) (1998) 1054–1057, https://doi.org/10.1103/PhysRevLett.81.1054.
[10] A.A. Karpushin, A.N. Sorokin, V.A. Gritsenko, Si–Si bond as a deep trap for electrons and holes in silicon nitride, JETP Lett. 103 (3) (2016) 171–174, https://doi.org/10.1134/S0021364016030085.
[11] V.A. Gritsenko, T.V. Perevalov, O.M. Orlov, G.Y. Krasnikov, Nature of traps responsible for the memory effect in silicon nitride, Appl. Phys. Lett. 109 (2016) 06294, https://doi.org/10.1063/1.4959830.
[12] Y.N. Novikov, V.A. Gritsenko, Charge transport mechanism and amphoteric nature of traps in amorphous silicon nitride, J. Non Cryst. Solids 544 (2020) 120186, https://doi.org/10.1016/j.jnoncrysol.2020.120186.
[13] Y.N. Novikov, V.A. Gritsenko, Multiphonon trap ionization mechanism in amorphous SiN_x, J. Non Cryst. Solids 582 (2022) 121442, https://doi.org/10.1016/j.jnoncrysol.2022.121442.
[14] M.E. Grillo, S.D. Elliott, J. Rodríguez, R. Añez, D.S. Coll, A. Suhane, L. Breuil, A. Arreghini, R. Degraeve, A. Shariq, V. Beyer, M. Czernohorsky, First-principles study of oxygen and aluminum defects in b-Si_3N_4: compensation and charge trapping, Comput. Mater. Sci. 81 (2014) 178–183, https://doi.org/10.1016/j.commatsci.2013.07.048.
[15] R.P. Vedula, N.L. Anderson, A. Strachan, Effect of topological disorder on structural, mechanical, and electronic properties of amorphous silicon nitride: an atomistic study, Phys. Rev. B 85 (2012) 205209, https://doi.org/10.1103/PhysRevB.85.205209.
[16] L.E. Hintzsche, C.M. Fang, T. Watts, M. Marsman, G. Jordan, M.W.P.E. Lamers, A. W. Weeber, G. Kresse, Density functional theory study of the structural and electronic properties of amorphous silicon nitrides: Si_3N_{4-x}:H, Phys. Rev. B 86 (2012) 235204, https://doi.org/10.1103/PhysRevB.86.235204.
[17] R.P. Vedula, S. Palit, M.A. Alam, A. Strachan, Role of atomic variability in dielectric charging: a first-principles-based multiscale modeling study, Phys. Rev. B 88 (2013) 205204, https://doi.org/10.1103/PhysRevB.88.205204.
[18] C. Wilhelmer, D. Waldhoer, T. Grasser, Over- and undercoordinated atoms as a source of electron and hole traps in amorphous silicon nitride (a-Si_3N_4), Nanomaterials 13 (2023) 2286, https://doi.org/10.3390/nano13162286.
[19] W.I. Choi, W.-J. Son, R. Dronskowski, Y. Oh, S.-Y. Yang, U. Kwon, D.S. Kim, Switchable chemical-bond reorganization for the stable charge trapping in amorphous silicon nitride, Adv. Mater. 36 (2024) 2308054, https://doi.org/10.1002/adma.202308054.
[20] V.A. Gritsenko, Silicon Nitride on Si: Electronic Structure for Flash memory Devices, in: V. Narayanan, M.M. Frank, A.A. Demkov (Eds.), Thin Films on Silicon Electronic and Photonic Applications, World Scientific Press, New Jersey, 2016, pp. 273–322.
[21] A. Goda, Recent progress on 3D NAND flash technologies, Electronics 10 (2021) 3156, https://doi.org/10.3390/electronics10243156.
[22] H.-D. Kim, H.-M. An, S.M. Hong, T.G. Kim, Forming-free SiN-based resistive switching memory prepared by RF sputtering a applications and materials science, Phys. Status Solidi A 210 (9) (2013) 1822–1827, https://doi.org/10.1002/pssa.201329021.
[23] A.A. Gismatulin, G.N. Kamaev, V.N. Kruchinin, V.A. Gritsenko, O.M. Orlov, A. Chin, Charge transport mechanism in the forming-free the memristor based on silicon nitride, Sci. Rep. 11 (2021) 2417, https://doi.org/10.1038/s41598-021-82159-7.
[24] T.-J. Yen, A. Chin, V.A. Gritsenko, Improved device distribution in high-performance SiNx resistive random access memory via arsenic ion implantation, Nanomaterials 11 (2021) 1401, https://doi.org/10.3390/nano11061401.
[25] H.J. Stein, Absorption edge and ion bombardment of silicon nitride, J. Appl. Phys. 47 (8) (1976) 3421, https://doi.org/10.1063/1.323177.
[26] G. Li, H. San, X.-Y. Chen, Charging and discharging in ion implanted dielectric films used for capacitive radio frequency microelectromechanical systems switch available to purchase, J. Appl. Phys. 105 (2009) 124503, https://doi.org/10.1063/1.3147862.
[27] P. Giannozzi, O. Andreussi, T. Brumme, et al., Advanced capabilities for materials modelling with quantum ESPRESSO, J. Phys. Condens. Mater 29 (46) (2017) 465901, https://doi.org/10.1088/1361-648X/aa8f79.
[28] R.D. Carson, S.E. Schnatterly, Valence-band electronic structure of silicon nitride studied with the of soft-x-ray emission, Phys. Rev. B 33 (4) (1986) 2432, https://doi.org/10.1103/PhysRevB.33.2432.

[29] O. Debieu, R.P. Nalini, J. Cardin, X. Portier, J. Perrière, F. Gourbilleau, Structural and optical characterization of pure Si-rich nitride thin flms, Nanoscale Res. Lett. 8 (2013) 31–36, https://doi.org/10.1186/1556-276X-8-31.
[30] R. Karcher, L. Ley, R.L. Johnson, Electronic structure of hydrogenated and unhydrogenated amorphous SiN_x ($0 \leq x \leq 1.6$): a photoemission study, Phys. Rev. 8 (30) (1984) 1896–1910, https://doi.org/10.1103/PhysRevB.30.1896.
[31] https://xpsdatabase.net/silicon-si-z14, (accessed 8 July 2025).
[32] I. Hoflijk, A. Vanleenhove, I. Vaesen, C. Zborowski, K. Artyushkova, T. Conard, HAXPES spectra of Si_3N_4 measured by Cr Kα, Surf. Sci. Spectra 29 (2022) 014013 https://doi.org/10.1116/6.0001524.
[33] F. Tiour, B. Benyahia, N. Brihi, A. Sari, B. Mahmoudi, A. Manseri, A. Guenda, Opto–structural properties of Si–rich SiN_x with different stoichiometry, Appl. Phys. A 126 (2020) 59, https://doi.org/10.1007/s00339-019-3258-5.
[34] L. Martín-Moreno, E. Martínez, J.A. Vergés, F. Yndurain, Electronic structure, defect states, and optical absorption of amorphous $Si_{1-x}N_x$ [$0 \leq x/(1-x) \leq 2$], Phys. Rev. B 35 (1987) 9683, https://doi.org/10.1103/PhysRevB.35.9683.
[35] J.F. Justo, F. de Brito Mota, A. Fazzio, First-principles investigation of a-SiN_x:H, Phys. Rev. B 65 (2002) 073202, https://doi.org/10.1103/PhysRevB.65.073202.
[36] O.V. Rambadey, A. Kumar, A. Sati, P.R. Sagdeo, Exploring the interrelation between urbach energy and dielectric constant in Hf-substituted $BaTiO_3$, ACS Omega 6 (2021) 32231–32238, https://doi.org/10.1021/acsomega.1c05057.
[37] G. Heinricha, I. Höger, M. Bähr, K. Stolberg, T. Wütherich, M. Leonhardt, A. Lawerenz, G. Gobsch, Investigation of laser irradiated areas with electron backscatter diffraction, Energy Procedia 27 (2012) 491–496, https://doi.org/10.1016/j.egypro.2012.07.099.
[38] H.H. Nguyen, R. Jayapal, N.S. Dang, V.D. Nguyen, T.T. Trinh, K. Jang, J. Yi, Investigation of charge storage and retention characteristics of silicon nitride in NVM based on InGaZnO channels for System-on-Panel applications, Microelectron. Eng. 98 (2012) 34–40, https://doi.org/10.1016/j.mee.2012.05.058.
[39] I. Guler, Characterization of N rich-silicon nitride thin films deposited by PECVD, ECS J. Solid State Sci. Technol. 12 (2023) 046002, https://doi.org/10.1149/2162-8777/acc971.
[40] https://refractiveindex.info/?shelf=main&book=Si&page=Schinke (accessed 1 September 2025).
[41] https://en.wikipedia.org/wiki/Silicon_nitride (accessed 1 September 2025).